Translational Oncology
www.transonc.com

Volume 11 Number xx pp. 504–510 504

Whole Tumor Histogram-profiling of Diffusion-Weighted Magnetic Resonance Images Reflects Tumorbiological Features of Primary Central Nervous System Lymphoma

Stefan Schob[*,1], Benno Münch[*,1], Julia Dieckow[*], Ulf Quäschling[*], Karl-Titus Hoffmann[*], Cindy Richter[*], Nikita Garnov[†], Clara Frydrychowicz[‡], Matthias Krause[§], Hans-Jonas Meyer[¶,1] and Alexey Surov[‖,1]

[*]Department for Neuroradiology, University Hospital Leipzig, Leipzig, Germany; [†]Eichamt Leipzig, Leipzig, Germany; [‡]Department for Neuropathology, University Hospital Leipzig, Leipzig, Germany; [§]Clinic for Neurosurgery, University Hospital Leipzig, Leipzig, Germany; [¶]Clinic for Diagnostic and Interventional Radiology, University Hospital Leipzig, Leipzig, Germany

Abstract

PURPOSE: Diffusion weighted imaging (DWI) quantifies motion of hydrogen nuclei in biological tissues and hereby has been used to assess the underlying tissue microarchitecture. Histogram-profiling of DWI provides more detailed information on diffusion characteristics of a lesion than the standardly calculated values of the apparent diffusion coefficient (ADC)—minimum, mean and maximum. Hence, the aim of our study was to investigate, which parameters of histogram-profiling of DWI in primary central nervous system lymphoma can be used to specifically predict features like cellular density, chromatin content and proliferative activity. *PROCEDURES*: Pre-treatment ADC maps of 21 PCNSL patients (8 female, 13 male, 28–89 years) from a 1.5T system were used for Matlab-based histogram profiling. Results of histopathology (H&E staining) and immunohistochemistry (Ki-67 expression) were quantified. Correlations between histogram-profiling parameters and neuropathologic examination were calculated using SPSS 23.0. *RESULTS*: The lower percentiles (p10 and p25) showed significant correlations with structural parameters of the neuropathologic examination (cellular density, chromatin content). The highest percentile, p90, correlated significantly with Ki-67 expression, resembling proliferative activity. Kurtosis of the ADC histogram correlated significantly with cellular density. *CONCLUSIONS*: Histogram-profiling of DWI in PCNSL provides a comprehensible set of parameters, which reflect distinct tumor-architectural and tumor-biological features, and hence, are promising biomarkers for treatment response and prognosis.

Translational Oncology (2018) 11, 504–510

Introduction

Primary central nervous system lymphoma (PCNSL) accounts for approximately 5% of all newly diagnosed brain tumors, predominantly affecting older patients [1]. It is a non-Hodgkin-lymphoma (NHL), strictly limited to the central nervous system (CNS), occurring in immuno-competent and immuno-compromised patients [2]. In approximately 90% of all manifestations, PCNSL are diffuse large B-cell type lymphomas [3]. Compared to other high-grade NHL outside the CNS, PCNSL is particularly aggressive and overall survival is poor. So far, management of PCNSL remains controversial and independent from the individual therapeutic approaches, disease recurrence is almost certain in the vast majority of patients [4]. The high recurrence rate of PCNSL is believed to reflect the peculiarity of the immune-privilege of the CNS, providing

Address all correspondence to: Stefan Schob, Department for Neuroradiology, University Hospital Leipzig, Liebigstraße 20, 04103 Leipzig.
E-mail: Stefan.Schob@Medizin.Uni-Leipzig.de
[1]Contributed equally.
Received 9 January 2018; Revised 16 February 2018; Accepted 16 February 2018

1936-5233
https://doi.org/10.1016/j.tranon.2018.02.006

a niche for the tumor cells, eventually resulting in minimal residual disease as a starting point for relapse [5].

Although PNCSL represents a rather rare CNS malignancy, a number of controlled trials have investigated promising cyto-reductive treatment regimens [6]. During recent years, whole brain radiation has been applied less frequently, since it bears almost no curative potential, although initial response to therapy is striking [7]. Multidrug-chemotherapy approaches, mostly based on methotrexate, are increasingly performed with beneficial outcomes. Results of complementary, non-methotrexate based chemotherapeutic approaches, for example in combination with autologous stem cell transplantation, might represent an effective alternative possibly associated with superior outcomes [5].

However, reliable, continuous non-invasive monitoring of response to anti-proliferative medication is becoming increasingly important for the oncologist to assess and compare efficacy of PCNSL treatments [8]. Cross sectional imaging, most importantly magnetic resonance imaging (MRI), has been shown to be of excellent accuracy regarding the diagnosis of intracranial lymphoma [9] and therefore is a propitious technique for this purpose. Although conventional MRI, including T2 weighted imaging, T1 weighted imaging, fluid attenuated inversion recovery (FLAIR) – imaging and gadolinium-enhanced imaging provides detailed information on localization, mass effect, blood brain barrier disruption, peri-focal edema and extent of infiltration of CNS mass lesions, it (very sensitively) visualizes only unspecific phenomena [10] and does not sufficiently reflect histopathological features of brain tumors [11].

Contrarily to conventional MRI, diffusion weighted imaging (DWI), a technique employing opposing gradients to visualize the motion of hydrogen nuclei on a microscopical scale, provides apparent diffusion coefficient (ADC) maps, which reflect microstructural features of biological tissues, and hence, can be employed as an imaging biomarker in various neoplastic conditions [12,13]. As an example, ADC values derived from small singular region of interest (ROI) measurements in pre-operative ADC maps of PCNSL patients, accurately representing the stereotactically biopsied specimen, precisely predicted the proliferative activity of the respective PCNSL manifestation [14].

However, the singular ROI method in the diagnostic pre-operative or follow-up setting has significant limitations, for example – inherent to the method – it cannot reflect features of the whole continuum of the space occupying lesion, and hence, tumor heterogeneity is not sufficiently depicted. Furthermore, inter-rater variability is another significant concern [15].

As a consequence, the aim of this study was to evaluate whether whole tumor histogram-profiling in preoperative ADC maps of PCNSL patients sufficiently reflects corresponding (immune-) histopathological properties like Ki-67 expression, cellular density and nuclear area, perspectively providing a sensitive tool for monitoring therapy-related changes of the tumor-architecture on a microscopical level.

Patients, Procedures and Methods

Patients Collective

Our radiological information system was searched for the diagnosis PCNSL. Twenty-one patients were finally included, all of which had confirmation by stereotactic biopsy and subsequent neuropathological workup in our hospital. The patients' collective was comprised of 8 female and 13 male subjects; ranging from 28 to 89 years with a mean age of 67.7 years. Informed consent was obtained in writing from all patients or caregivers for the asservation of sample remnants and compiling of clinical and radiological data. The study was approved by the local ethics committee (Ethikkommission Universität Leipzig, Az 330-13-18112013). Requirements for the study were sufficient pretreatment MRI scans including DWI. MRI examinations of the included patients did not reveal signs of hemorrhage or calcifications.

MRI specifics

All images were acquired in the clinical diagnostic routine using a 1.5Tesla MRI system (Siemens Magnetom Symphony 1,5T) with the standard Siemens head coil (CP head array, model #1P3146037). DWI was performed using a single shot echo planar sequence with following parameters: Echo time(TE)/Repetition time(TR) = 6000/105 ms, 90° flip angle, 57 transverse sections, slice thickness = 5 mm, field of view (FOV) = 230 mm. Diffusion-sensitizing gradients were applied sequentially in the x, y and z directions with b factors of 0 and 1000 s/mm2. ADC maps were then automatically generated by the operating console of the MR scanner. Postcontrast T1-weighted 3D-gradient echo sequence(GRE) imaging was obtained with following parameters: TR/TE = 2150/3.93 ms, flip angle 15°, 1-mm section thickness and 230 mm FOV. A standard dose (0.1 mmol/kg body weight) of gadolinium based contrast agent (Gadovist, Bayer, Leverkusen, Germany) was injected intravenously. Routine anatomic precontrast T1/T2_tirm_tra_dark_fluid (TR/TE = 9000/114, slice thickness 5mm, flip angle 150°, 28 transverse sections) images were also obtained.

All images were available in digital form and analyzed by one experienced radiologist (SS) without knowledge of the histopathological diagnosis on a PACS workstation (syngo.plaza VB20, Siemens, Germany).

Histogram Profiling of ADC Maps

ADC maps and T1weighted post contrast images were exported from our radiological archive in DICOM format *via* the aforementioned Siemens PACS. Using a custom-made DICOM image analysis tool (programmed by N.G. using Matlab, The Mathworks, Natick, MA), whole tumor diffusion profile analysis *via* the histogram approach was performed as follows; T1weighted post-Gadolinium images were displayed in a graphical user interface (GUI) to tag the contrast-enhancing tumor of each patient in all respective MRI sections. All drawn regions of interest (ROIs) were then automatically propagated onto the corresponding ADC maps and the whole lesion histogram profile was consecutively calculated, providing the following set of parameters: ADCmean, ADCmin, ADCmax, ADCp10, ADCp25, ADCp75, ADCp90, ADCmodus, ADCmedian, Skewness, Kurtosis, and Entropy.

Neuropathology

All tumor specimens were used for neuro-histological confirmation of the diagnosis. A 5µm section of each tumor was stained by H&E and a further section was employed for Ki-67 immunohistochemistry to determine the proliferation rate [14], as previously reported.

The (immune-) histopathological images were digitalized with a Jenalumar microscope, carrying a 4.2 digital camera (Zeiss, Jena, Germany). Thereupon, Ki-67 index, cell count, average nuclear area and total nuclear area of each specimen were quantified using the ImageJ particles tool [16] as described previously.

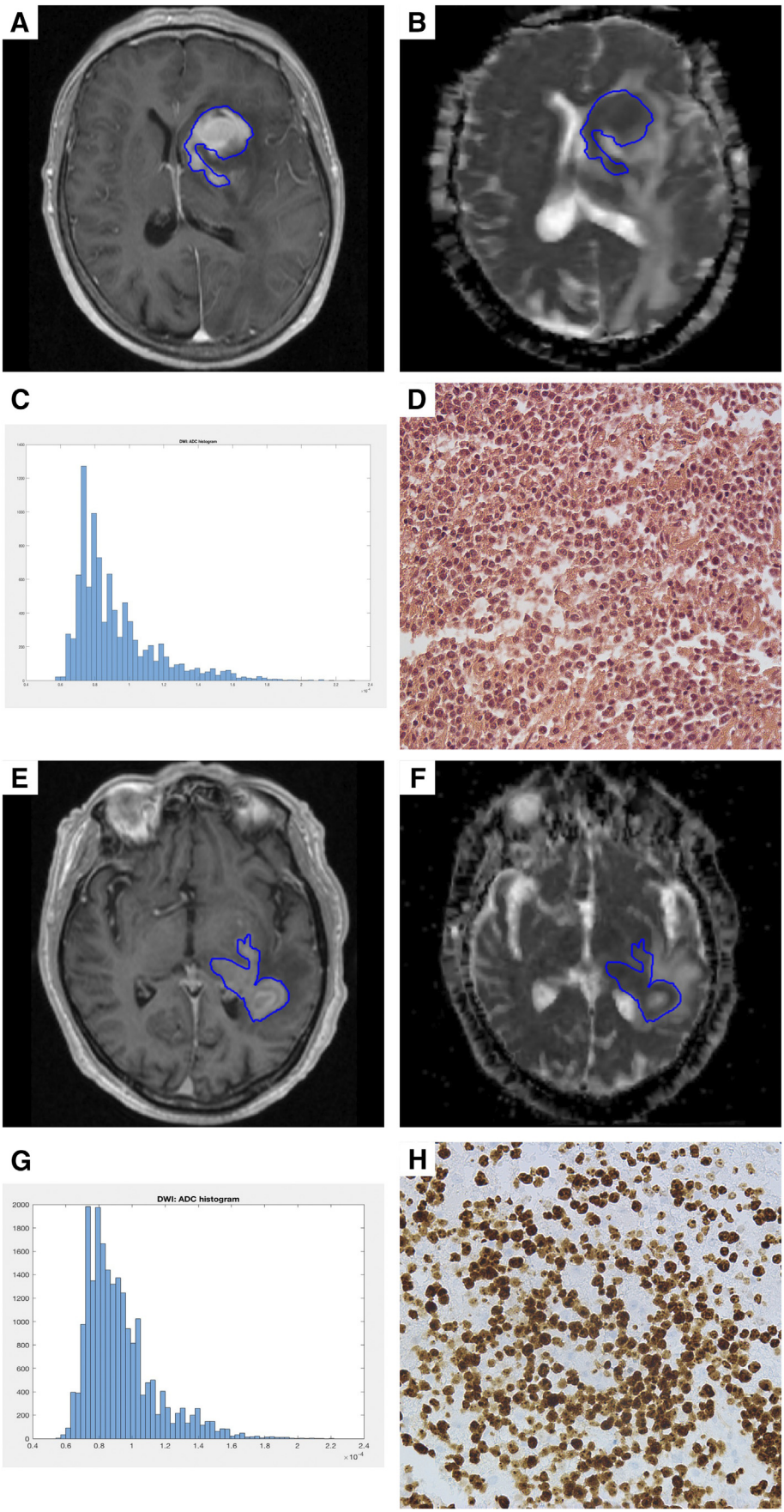

Figure 1. MR-Imaging, Ki-67 staining and ADC histograms of two exemplary PCNSL patients. A-D and E-H show two examples of PCNSL. A and E are giving the T1 post contrast images of both individuals, B and F display the corresponding section of the ADC map. C and F show the respective ADC histograms. D and H represent Ki-67 staining of the biopsy specimen.

Table 1. DWI Histogram Profiling and Neuropathologic Parameters of All Investigated PCNSL

Parameters	Mean ± Standard Deviation	Minimum	Maximum
ADC_{mean}, × 10^{-5} mm^2s^{-1}	98.56 ± 16.49	73.02	137.55
ADC_{min}, × 10^{-5} mm^2s^{-1}	57.45 ± 19.40	13.37	92.11
ADC_{max}, × 10^{-5} mm^2s^{-1}	190.49 ± 48.22	86.54	313.53
P10 ADC, × 10^{-5} mm^2s^{-1}	77.16 ± 13.49	54.81	106.70
P25 ADC, × 10^{-5} mm^2s^{-1}	85.34 ± 15.76	60.09	120.20
P75 ADC, × 10^{-5} mm^2s^{-1}	109.95 ± 19.85	75.33	157.38
P90 ADC, × 10^{-5} mm^2s^{-1}	125.19 ± 21.75	76.18	172.29
Median ADC, × 10^{-5} mm^2s^{-1}	95.88 ± 18.18	72.40	137.29
Mode ADC, × 10^{-5} mm^2s^{-1}	90.68 ± 22.50	55.34	140.30
Kurtosis	4.72 ± 3.05	2.17	14.63
Skewness	0.85 ± 0.77	-0.42	2.51
Entropy	4.22 ± 0.69	2.79	5.55
Cell count, n	1288.62 ± 366.69	319	1922
Total Nuclear Area, µm	106617.71 ± 44549.13	19988.01	216517.76
Average Nuclear Area, µm	86.49 ± 46.41	53.20	267.91
Ki-67, %	76.19 ± 12.54	50.0	95.0

Statistical Analysis

Statistical analysis including graphics creation was performed using SPSS 23.0 (SPSS Inc, Chicago, IL).

Firstly, DWI histogram profile information and (immune-) histopathological data were investigated using descriptive statistics. Secondly, data was tested for Gaussian distribution using the Shapiro-Wilk Test. Finally, correlation analysis for normally distributed parameters was performed using Pearson Correlation Coefficient. In case of non-Gaussian distribution, Spearman-Rho Rank-Order Correlation was performed. $P < .05$ was taken to indicate statistical significance in all instances.

Results

Two examples of cranial MRI including the corresponding whole-tumor ADC-histograms and Ki-67 stainings from patient suffering from PCNSL are given in Figure 1).

The results of the descriptive analysis on DWI data and histopathological information are summarized in Table 1). Shapiro-Wilk-Test revealed Gaussian distribution for ADCmean, ADCmin, ADCmax, ADCp10, ADCp25, ADCp75, ADCp90, ADCmodus, ADCmedian, Skewness, Entropy, cell count, total nuclear area and Ki-67 (data not shown). Non-Gaussian distribution was determined for Kurtosis and average nuclear area (data not shown).

Pearson's correlation coefficient was used to investigate the association between ADCmean, ADCp10, ADCp25, ADCp75, ADCp90, ADCmodus, ADCmedian, Skewness, Entropy, cell count, total nuclear area and Ki-67. Spearman-Rho Rank-Order Correlation was calculated to investigate the association between Kurtosis, cell count, average nuclear area, total nuclear area and Ki-67. Also, correlations between average nuclear area and all evaluated DWI histogram data were calculated using Spearman-Rho Rank-Order. Significant correlations were identified for the following pairs of parameters; ADCmean and Ki-67 (r = –0.434, p = 0.049), ADCmean and total nuclear area (r = -0.462, p = 0.035), ADCp10 and cell count (r = -0.435, p =0.049), ADCp10 and total nuclear area (r = -0.455, P = .038), ADCp25 and total nuclear area (r = -0.458, , P = .037) ADCp90 and Ki-67 (r = -0.439, , P = .047), Kurtosis and cell count (r = 0.458, , P = .037). The results of the correlative analysis are summarized in Table 2). Figure 2) is showing the identified significant correlations as dot plots.

Discussion

In this study we aimed to investigate, whether whole tumor ADC histogram-profiling sufficiently reflects microscopical tumor-architecture and proliferative activity of PCNSL.

To our best knowledge, this work is the first showing statistically significant associations between ADC histogram-profiling parameters and prognostically relevant (immune-)histopathological features in a collective of PCNSL patients.

In detail, kurtosis of the whole tumor ADC histogram correlated with cellular density of the investigated PCNSL, indicating that increased kurtosis reflects high cellularity in this specific malignant neoplastic CNS lesion. This finding conforms with the results of a recently published investigation of malignant tumors in the thyroid

Table 2. Correlations of DWI-Histogram Profile Parameters with Cellular Density, Total Nuclear Area and Average Nuclear Area as Well as Ki-67 in All Investigated PCNSL

DWI Histogram Profile Parameters	Cell Count (n)	Total Nuclear Area (μm^2)	Average Nuclear Area (μm^2)	Ki-67 (%)
ADC_{mean}, × 10^{-5} mm^2s^{-1}	r = -0.390	r = -0.462	r = - 0.254	r = -0.434
	P = .080	P = .035	P = .267	P = .049
ADC_{min}, × 10^{-5} mm^2s^{-1}	r = -0.275	r = -0.338	r = -0.289	r = -0.223
	p=0.228	P = .135	P = .204	P = .332
ADC_{max}, × 10^{-5} mm^2s^{-1}	r = 0.200	r = -0.048	r = -0.153	r = -0.373
	P = .386	P = .835	P = .597	P = .096
ADCp10, × 10^{-5} mm^2s^{-1}	r = -0.435	r = -0.455	r = - 0.234	r = -0.409
	P = .049	P = .038	P = .308	P = .066
ADCp25, × 10^{-5} mm^2s^{-1}	r = -0.400	r = -0.458	r = -0.255	r = - 0.380
	P = .072	P = .037	P = .264	P = .089
ADCp75, × 10^{-5} mm^2s^{-1}	r = -0.368	r = -0.406	r = -0.202	r = -0.388
	P = .100	P = .068	P = .381	P = .082
ADCp90, × 10^{-5} mm^2s^{-1}	r = -0.343	r = -0.411	r = -0.202	r = -0.439
	P = .128	P = .064	P = .379	P = .047
ADCMedian, × 10^{-5} mm^2s^{-1}	r = -0.368	r = -0.419	r = -0.235	r = -0.363
	P = .100	P = .059	P = .306	P = .106
ADCModus, × 10^{-5} mm^2s^{-1}	r = -0.256	r = -0.373	r = -0.265	r = -0.232
	P = .262	P = .096	P = .245	P = .311
Kurtosis	r = -0.458	r= 0.175	r = -0.136	r = 0.035
	P = .037	P = .448	P = .558	P = .882
Skewness	r = 0.338	r = 0.201	r = -0.001	r = -0.036
	P = .134	P = .383	P = .998	P = .876
Entropy	r = 0.053	r = -0.023	r = 0.067	r = -0.263
	P = .820	P = .923	P = .774	P = .248

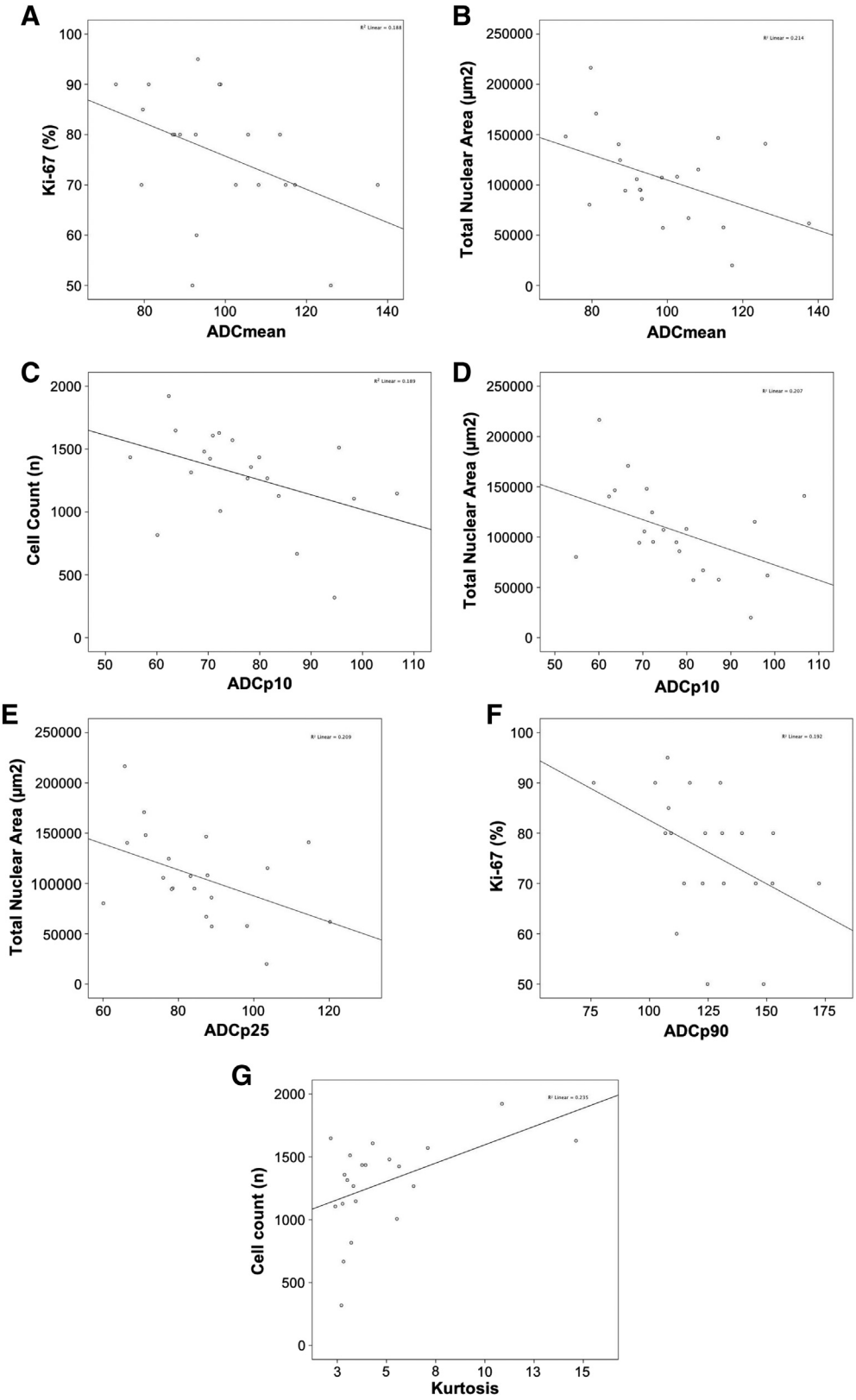

Figure 2. Identified correlations between immune-histopathological parameters and whole-tumor ADC-profiling. ADCmean values correlate with Ki-67 expression and average nuclei area. The lower percentiles, p10 and p25 correlate with structural parameters of the histopathological analysis – cell count and average nuclei area. P90, contrarily, only correlates with Ki-67 expression. The peakedness of the ADC histogram – kurtosis – correlates with cell count.

gland, showing that cellularity in thyroid carcinoma is associated with kurtosis of the whole tumor ADC histogram [17]. Our findings are further corroborated by the study of Kyriazi et al. [18], who were able to demonstrate that changes in ADC histogram kurtosis correlate with response to cyto-reductive chemotherapy in metastatic ovarian and primary peritoneal cancer, as well as with the study of Foroutan et al. [19], who demonstrated early changes in ADC histogram kurtosis as a sign of response to anti-proliferative treatment in a xenotransplant model of osteosarcoma.

Interestingly, skewness and entropy of the whole tumor ADC histogram were not significantly correlated with (immune-) histopathological features in our investigation. Other malignant entities – for example cervical carcinomas, however, revealed correlations between entropy and skewness of ADC histograms and histopathological features, which is probably a consequence of the distinct cellular- and matrix-architecture of the respective tumors, which are composed of a stromal and an epithelial compartment, other than the typically very homogeneous PCNSL [20,21].

Additionally, the lower percentiles of whole tumor diffusion profiling (p10 and p25) showed significant correlations with measures of cellularity and chromatin content, features representing tumor viability and progression. This result is underlined by a previous work investigating uterine cervical carcinomas with and without metastatic dissemination [20]. This study revealed significantly different values in the tenth percentile of whole tumor ADC values when comparing manifestations of the disease, which already had gained the ability to spread metastatically with non-metastasized manifestations. Our findings further coincide with the earlier work of Kyriazi and coworkers, which demonstrated changes in ADC p10 values as an expression of response to chemotherapy in ovarian and peritoneal cancer [18].

The ninetieth percentile of whole tumor diffusion profiling (p90) showed a statistically significant, inverse correlation with the expression of Ki-67, a nuclear protein being only detectable during active proliferation [22]. An almost identical correlation was identified in thyroid carcinomas, as published previously [17]. This, so far, suggests a specific sensitivity of the 90th percentile for the reflection of the proliferative activity of malignant tumors.

In concordance with the results of our previously published study, which used a singular ROI for ADC quantification [14], mean values of whole tumor diffusion profiling did correlate significantly with Ki-67 expression and total nuclear area, representing surrogate markers for active proliferation and chromatin content in the tumor. The mean value of ADC quantification obtained *via* both, the whole lesion and the singular-one-slice ROI approach, has been demonstrated to very well reflect cellularity and proliferative activity in different malignant conditions [23], even though singular ROIS are significantly less accurate than the whole lesion approach [15]. However, the mean value of ADC quantification as a singular parameter cannot sufficiently provide a whole spectrum of information about the complexity of the micro-architecture of a neoplastic tissue, but rather creates a significantly filtered and condensed approximation.

Thus we conclude that whole tumor ADC histogram profiling, giving a comprehensible number of different parameters that relatively specifically reflect different aspects of clinical relevant tumor biology, is a very useful extension of the commonly employed singular ROI technique.

Our study suffers from some limitations. Firstly, it is only a retrospective study and confined to a small quantity of PCNSL patients. Secondly, the study did not include 3T images and therefore is only representative for the lower magnetic field strength. Furthermore, comparability of the obtained values between different 1.5T scanners is still uncertain and must be validated in further investigations.

Conclusions

Whole tumor histogram-profiling of ADC maps provides a comprehensible set of parameters, which are very useful for pre-treatment estimation of tumor biological properties of PCNSL. The technique is a promising candidate for a non-invasively obtained biomarker, probably allowing for sensitive and specific estimation of tumor response to cyto-reductive treatment regimens. However, further prospective studies are warranted to validate our findings.

Conflict of interest

The authors declare no conflict of interest.

Acknowledgments

This study was supported by the Clinician Scientist Program of the Medical Faculty of the University Leipzig.

References

[1] Tang YZ, Booth TC, Bhogal P, Malhotra A, and Wilhelm T (2011). Imaging of primary central nervous system lymphoma. *Clin Radiol* **66**, 768–777.

[2] Batchelor T and Loeffler JS (2006). Primary CNS lymphoma. *J Clin Oncol* **24**, 1281–1288.

[3] Gerstner ER and Batchelor TT (2011). Primary Central Nervous System Lymphoma. Primary Central Nervous System Tumors. Totowa, NJ: Humana Press; 2011. p. 333–353.

[4] Visagan MR, Cheserem MB, Stapleton MS, Bridges DL, and Eralil MG (2017). PP78. Primary CNS Lymphoma Outcomes in a Single Centre: A 7 Year Study. *Neuro-Oncology* **19**, i21.

[5] Schorb E, Finke J, Ferreri AJM, Ihorst G, Mikesch K, Kasenda B, Fritsch K, Fricker H, Burger E, and Grishina O, et al (2016). High-dose chemotherapy and autologous stem cell transplant compared with conventional chemotherapy for consolidation in newly diagnosed primary CNS lymphoma—a randomized phase III trial (MATRix). *BMC Cancer* , 1–9.

[6] DeAngelis L and Neuro-oncology M (2015). Primary CNS lymphoma treatment —the devil is in the details. *Nature Publishing Group*, 1–2.

[7] Fallah J, Qunaj L, and Olszewski AJ (2016). *Therapy and outcomes of primary central nervous system lymphoma in the United States: analysis of the National Cancer Database. Blood Advances* **1**, 112–121.

[8] Wieduwilt MJ, Valles F, Issa S, Behler CM, Hwang J, McDermott M, Treseler P, O'Brien J, Shuman MA, and Cha S, et al (2012). *Immunochemotherapy with intensive consolidation for primary CNS lymphoma: a pilot study and prognostic assessment by diffusion-weighted MRI. Clin Cancer Res* **18**, 1146–1155.

[9] Haldorsen IS, Espeland A, and Larsson EM (2011). *Central nervous system lymphoma: characteristic findings on traditional and advanced imaging. American Journal of Neuroradiology* **32**, 984–992.

[10] Upadhyay N and Waldman AD (2011). *Conventional MRI evaluation of gliomas. BJR* **84**(2), S107–S111.

[11] Schob S, Frydrychowicz C, Gawlitza M, Bure L, Preuss M, Hoffmann K-T, and Surov A (2016). *Signal Intensities in preoperative MRI do not reflect proliferative activity in meningioma. Translational Oncology* **9**, 274–279.

[12] Padhani AR, Liu G, Mu-Koh D, Chenevert TL, Thoeny HC, Takahara T, Dzik-Jurasz A, Ross BD, Van Cauteren M, and Collins D, et al (2009). *Diffusion-weighted magnetic resonance imaging as a cancer biomarker: consensus and recommendations. Neoplasia* **11**, 102–125.

[13] Le Bihan D (2013). *Apparent diffusion coefficient and beyond: what diffusion MR imaging can tell us about tissue structure. Radiology* **268**, 318–322.

[14] Schob S, Meyer J, Gawlitza M, Frydrychowicz C, Müller W, Preuss M, Bure L, Quäschling U, Hoffmann K-T, and Surov A (2016). *Diffusion-weighted MRI reflects proliferative activity in primary CNS lymphoma. PLoS ONE* **11** e0161386.

[15] Ahn SJ, Shin HJ, Chang J-H, and Lee S-K (2014). *Differentiation between primary cerebral lymphoma and glioblastoma using the apparent diffusion coefficient: comparison of three different ROI methods. PLoS ONE* **9** e112948.

[16] Surov A, Caysa H, Wienke A, Spielmann RP, and Fiedler E (2015). *Correlation between different ADC fractions, cell count, Ki-67, total nucleic areas and average nucleic areas in meningothelial meningiomas. Anticancer Res* **35**, 6841–6846.

[17] Schob S, Meyer H, Dieckow J, Pervinder B, Pazaitis N, Höhn A, Garnov N, Horvath-Rizea D, Hoffmann K-T, and Surov A (2017). *Histogram analysis of diffusion weighted imaging at 3t is useful for prediction of lymphatic metastatic spread, proliferative activity, and cellularity in thyroid cancer. IJMS* **18**, 821–912.

[18] Kyriazi S, Collins DJ, Messiou C, Pennert K, Davidson RL, Giles SL, Kaye SB, and de Souza NM (2011). *Metastatic ovarian and primary peritoneal cancer: assessing chemotherapy response with diffusion-weighted MR imaging—value of histogram analysis of apparent diffusion coefficients. Radiology* **261**, 182–192.

[19] Foroutan P, Kreahling JM, Morse DL, Grove O, Lloyd MC, Reed D, Raghavan M, Altiok S, Martinez GV, and Gillies RJ (2013). *Diffusion MRI and novel texture analysis in osteosarcoma xenotransplants predicts response to anti-checkpoint therapy. PLoS ONE* **8** e82875.

[20] Schob S, Meyer HJ, Pazaitis N, Schramm D, Bremicker K, Exner M, Höhn A-K, Garnov N, and Surov A (2017). *ADC histogram analysis of cervical cancer aids detecting lymphatic metastases—a preliminary study. Mol Imaging Biol* **61**, 69.

[21] Just N (2014). *Improving tumour heterogeneity MRI assessment with histograms. Br J Cancer* **111**, 2205–2213.

[22] Tisell LE, Oden A, Muth A, Altiparmak G, Mölne J, Ahlman H, and Nilsson O (2003). *The Ki67 index a prognostic marker in medullary thyroid carcinoma. Br J Cancer* **89**, 2093–2097.

[23] Chen L, Liu M, Bao J, Xia Y, Zhang J, Zhang L, Huang X, and Wang J (2013). *The correlation between apparent diffusion coefficient and tumor cellularity in patients: a meta-analysis. PLoS ONE* **8** e79008.